Published in final edited form as:
Anal Chem. 2009 January 1; 81(1): 369–377. doi:10.1021/ac8016532.

A Combined Charged Residue-Field Emission Model of Macromolecular Electrospray Ionization

Christopher J. Hogan Jr.*[1,4], **James A. Carroll**[3], **Henry W. Rohrs**[2], **Pratim Biswas**[1], and **Michael L. Gross**[2]

1*Department of Energy, Environmental, & Chemical Engineering, Washington University in St. Louis, MO, USA*

2*Department of Chemistry, Washington University in St. Louis, MO, USA*

3*Pfizer Global Research & Development, Saint Louis, MO, USA*

4*Department of Mechanical Engineering, Yale University, New Haven, CT, USA*

Abstract

The mechanism of the multiple charging of macromolecules in electrospray ionization (ESI) continues to inspire debate and controversy. Recently, we proposed that the number of charges on a macromolecule is determined by the emission of small charge carriers from macromolecule-containing nanodroplets and that, after solvent evaporation, the remaining charge is transferred to the macromolecule. In this study, we tested the applicability of this new theory for macromolecular, positive-ion ESI mass spectrometry by measuring the mean charge states and charge distributions of globular proteins under non-denaturing and denaturing conditions. Predictions of protein mean charge states for native state proteins are in excellent agreement with mass spectrometric measurements, giving strong credence to the proposed theory. Theoretical predictions are also in good agreement with mean charge states measured for proteins in basic solutions (pH = 11.5). For some proteins in acidic solutions (pH = 2.1), the measured mean charge states are anomalously higher than the Rayleigh limit of a water droplet with a volume equivalent to that of the protein. We propose that some macromolecules that are highly charged in solution may desorb from charged droplets of the same polarity in a similar manner to that whereby charge carriers emit from nanodroplets, leading to “supercharged” macromolecular ions. Examination of rate expressions for solvent evaporation and charge-carrier emission demonstrates that the newly proposed model for ESI is consistent with previously reported ion-emission kinetics. Overall, we obtained additional experimental evidence for the charge carrier emission model for macromolecular charging, suggesting opportunities for understanding and applying ESI-MS.

Keywords

Electrospray Ionization; Macromolecules; Mass Spectrometry; Ion Emission; Nanodroplets

INTRODUCTION

Electrospray ionization (ESI) is the most frequently used method to produce gas-phase macromolecular ions (e.g., of proteins, nucleic acids, industrial polymers) for mass

Correspondence to: Christopher J. Hogan, Jr.*.

To whom correspondence should be addressed: Tel: 203-432-4353; Fax: 203-432-7654 email: Christopher.Hogan@yale.edu.

spectrometry (MS). It is unique among ionization techniques in that it produces multiply charged gas-phase macromolecular ions[1], whereas other ionization techniques[2] typically produce singly charged ions. Because the ions are multiply charged, analytes with molecular masses of hundreds of kDa can be introduced into the gas phase with mass-to-charge (*m/z*) ratios well within the range of contemporary mass spectrometers[3]. Multiple charging is, therefore, one key feature of ESI that makes its use commonplace.

Two competing mechanisms explain how macromolecules become multiply charged in ESI, the charged-residue mechanism (CRM)[4, 5] and the ion-emission mechanism (IEM)[6]. According to the CRM, the excess charges on ESI droplets are transferred to and remain on macromolecules enclosed within the droplets after solvent evaporation. The charge on a macromolecule is limited by the maximum charge (i.e., the Rayleigh limiting charge) that a droplet similar in size to the macromolecule can contain without fissioning[5]. Conversely, according to IEM theory[7-10], analyte ions desorb directly from charged nanodroplets, driven by the large electric field at the droplet surface[11-17]. The formation of low molecular weight, singly charged ions in ESI has been explained well by the IEM[18]. Despite extensive study of macromolecular ESI[6, 19-22], neither mechanism explains quantitatively the extent of macromolecular multiple charging. We do know, however, that the extent of multiple charging depends on the molecular weight (i.e., size) of ionized the macromolecules[5, 23] and on their conformation (e.g., native-state proteins electrosprayed at neutral pH typically have lower charge states than do denatured proteins electrosprayed from acidic solutions[24-29]). Clearly, the charge-state distribution of macromolecular ions relates directly to the physicochemical properties of electrosprayed macromolecules. Therefore, an understanding of the mechanism of multiple charging of macromolecules in ESI is of great interest, and the ability to predict charge-state distributions would enhance the amount of information attainable from macromolecular mass spectrometry[26].

Recently, we presented a theory of macromolecular ESI[30] in which macromolecules are charged residues, but their charge state is determined by the field emission of charged ions from highly charged droplets[15, 31, 32]. This theory, which combines aspects of both the CRM and the IEM, has been strongly supported by gas-phase, ion mobility measurements[33-35] and mass spectrometry of native-state proteins, and it can be used to predict the number of charges on an electrosprayed macromolecule. Here, we present an expanded analysis, addressing ESI of proteins in their native states, in solutions containing mixed electrolytes, and in strongly acidic and basic solutions. We first describe the mechanism of macromolecular ESI, then compare theoretical predictions with experimental results, and finally discuss the implications of the proposed theory for both protein and small molecule ESI-MS.

THEORY OF MACROMOLECULAR ESI

Evaporation and Coulombic fissions[36] of ESI droplets eventually give rise to highly charged droplets, several tens of nanometers in diameter, some of which contain a single macromolecule[37]. The droplets carry excess positive charge on their surface when the emitter is positively charged, which is usually the case for most applications of macromolecular ESI-MS. We assume that most of the excess charge is carried by solvated ions and protons, as opposed to the macromolecule itself, which remains solvated inside the droplet. Once evaporation of solvent and volatile electrolyte ceases, the residual excess charge is transferred to the macromolecule. The charge state of macromolecules is not controlled by the Rayleigh limit of a droplet of similar size to the macromolecule, as it is in the CRM, but rather by the extent of ion emission from the droplet. The electric field on the surface of a charged droplet is inversely proportional to the square of the droplet diameter[15]. For a nanodroplet, the electric field strength can reach values as high as several V nm^{-1}, sufficient to drive the emission of excess charge-carrying ions from the droplet[16, 17, 32, 38].

The emission of an ion from a droplet occurs only when the electric field strength at the droplet surface is of a critical value E^*. Once an ion emits from the droplet, the electric-field strength at the surface decreases, which prevents further ion emission until the electric field again increases, by neutral solvent evaporation, to E^*. Ion emission and solvent evaporation both occur almost concurrently on rapid time scales, such that the electric-field strength at the droplet surface remains approximately constant and close to E^* as the droplet grows smaller. Thus, the number of charges, n, on an ion-emitting droplet of diameter D can be calculated from the equation:

$$n = \left[\frac{\pi \varepsilon_0 E^* D^2}{e}\right] \quad (1)$$

where ε_0 is the permittivity of free space and e is the unit electron charge. Equation [1] predicts that the number of charges on an ion-emitting droplet is proportional to the square of the droplet's diameter (i.e., proportional to its surface area). Likewise, as solvent evaporation approaches completion, a macromolecule present in it can accommodate remaining excess charges; thus, a macromolecular ion of surface area equivalent diameter, D, should also have n charges[39]. Macromolecules in droplets produced by ESI presumably exhibit a variety of conformations and have a distribution of diameters[40, 41], giving rise to the distribution of charges observed for macromolecular ions in ESI-MS . If a macromolecule's average diameter is used in equation [1], then the calculated n is representative of the average charge state for a type of macromolecular ion produced by ESI.

The number of charges on a macromolecule will also be directly proportional to E^*, the electric-field strength at which ion emission occurs. E^*, in turn, is dependent on the solvation energies[42] of the charge carriers within a charged droplet. In a series of studies utilizing ion mobility and mass analysis, Fernandez de la Mora and coworkers[13, 15, 31, 43] showed that ions of ionic liquids, metal salts, and ammonium salts are emitted from highly charged nanodroplets. For all the examined salts and ionic liquids, more than one type of ion was detected whose formation was determined to be through ion emission (e.g., for an ionic compound A^+B^-, A^+, $A^+(AB)$, and $A^+(AB)_x$ with x up to 4 are formed by ion emission. Gas-phase ions formed through direct emission from a charged droplet are presumably present on the droplet's surface as excess charge carriers prior to being emitted[44]. Electrolytes, typically added to protein solutions for ESI experiments, will carry excess droplet charge and gas-phase ions of electrolytes may form ions by field emission. Likewise, any impurities present in solution (e.g., Na^+) may also carry charge on electrospray droplet surfaces. Proposing that electrolytes form surface clusters with themselves or with impurities in solution, we note that charge carriers with different solvation energies will be present. The least solvated charge carrier, with the lowest E^*, requires the least activation energy for ion emission and will be preferentially emitted over all other charge carriers, until it is no longer present on the droplet surface. After the droplet is depleted of the least solvated charge carrier, neutral solvent evaporation occurs, increasing the electric-field strength at the droplet surface, and a new charged species, with a higher E^*, will be emitted from the droplet (i.e., charged species are released from droplets in order of least solvated to most solvated[45]). Therefore, with the use of some electrolytes, the droplet charge during ion emission will be directly proportional to a particular E^* value for a certain range of diameters, but E^* may shift to larger values for smaller droplets.

The dynamics of charge emission from an evaporating, charged nanodroplet and the resulting charge on a macromolecule within the nanodroplet are shown schematically in Figure 1. A macromolecule-containing nanodroplet has its excess charge carried by two different species, AH^+ and BH^+. If BH^+ is the less solvated of the two charge carriers, it emits first and at a lower E^* than AH^+. Once the droplet is depleted of BH^+, AH^+ emits, but only after the droplet surface electric field strength reaches a higher value, produced by neutral solvent evaporation. As

solvent evaporation nears completion, the reaction $AH^+(soln) \rightarrow A(g) + H^+(soln)$ at the macromolecular surface, providing protons to charge the macromolecule. The graph in the upper right of Figure 1 shows the hypothetical droplet charge versus droplet diameter curve for an ion-emitting droplet with two charge carriers. In regions where ion emission is occurring, the droplet charge is related to the droplet diameter by equation 1. When E^* shifts, however, no ion emission occurs, and the droplet charge remains constant.

EXPERIMENTAL & CALCULATION METHODS

Protein Charge States

A test of the proposed theory requires measurement of the charge-state distributions as well as the diameters of macromolecules at the moment solvent evaporation ceases. Charge-state distributions of native-state and denatured globular proteins were determined by using ESI quadrupole-time-of-flight MS with a Q-TOF Micro (Micromass, Mancheser, UK). Samples were introduced to the mass spectrometer by using direct infusion ESI at a flow rate of 5 μL min^{-1}. Dry N_2 gas at a flowrate of 50 L min^{-1} and a temperature of 50°C was used to desolvate the proteins; the temperature was kept low to minimize denaturation in the ion source[46]. All applied voltages at the mass spectrometer source were kept constant for all mass spectral measurements[3]. Positive-ion ESI was used for all measurements, and data for each mass spectrum were collected for 10 min.

Native-state protein measurements were made by using aqueous 10 mM ammonium acetate (NH_4Ac, pH = 6.7) and 10 mM triethyl ammonium bicarbonate (TEAB, pH = 7.3), as well as a mixture of 5 mM NH_4Ac and 5 mM TEAB. Mass spectra were also measured for proteins in 2 M aqueous acetic acid (HAc, pH = 2.1) and 2 M ammonium hydroxide (NH_4OH, pH = 11.5). Proteins with molecular weights ranging from 5.8 kDa (insulin) up to 76 kDa (holotransferrin) were measured. The average charge state was determined by numerical integration over all the peaks in the mass spectrum and subsequent calculation of their centroid[25]. The standard deviation of the charge state distribution in each mass spectrum was similarly calculated.

All proteins and chemicals were purchased from Sigma-Aldrich (St. Louis, MO) and used without additional purification.

Protein Diameter

A series of diameter measurements were previously made for native state globular proteins[33, 34, 47] by charge reduction electrospray size spectrometry[48, 49]. The technique utilizes electrospray ionization to aerosolize proteins from non-denaturing solutions. Following electrospray ionization, bipolar charging is used bring the droplets and subsequently the proteins to a steady-state Fuchs charge distribution[50], in which most protein aerosol particles are uncharged, and the small fraction of protein aerosol particles that remain charged are predominantly singly charged[51]. The electrical mobility distribution of the protein aerosol particles is then measured and then used to infer the protein diameter distribution. Previous measurements clearly show that the diameter of globular proteins in the gas phase is directly proportional to the $1/3^{rd}$ power of the protein molecular weight[33, 34]. It was noted, however, that the average gas-phase protein density calculated from such measurements, 0.57 g cm^{-3}, is unreasonably low[30, 52] for solvent-free, gas-phase protein ions. An explanation is that globular proteins are not perfectly spherical and residual electrolyte and/or solvent is present on protein aerosol particles[53, 54]. Electrolyte and solvent clustering is usually not seen in ESI-MS owing to designed declustering in the ion source[55], but residual electrolyte and solvent could give rise to larger than expected protein diameters in mobility-based measurements. Nevertheless, electrospray is used for protein aerosolization in both ion mobility and analytical

MS, providing an explanation for the reasonable agreement between different laboratories that determined protein diameters[56]. Thus, the measured diameters of gas-phase protein macromolecules introduced by electrospray ionization should be reasonable estimates of their sizes at the point at which ion emission ceases in ESI. Given the ambiguity in previous measurements and lack of a mobility standard for protein-sized particles[56-58], however, the accuracy of mobility measurements is uncertain. Future mobility measurements, made with high resolution instrumentation[59], combined with calculations of the theoretical protein ion collision cross sections[60] will be necessary to resolve the issue of gas-phase protein density. Furthermore, if ion emission also occurs concurrently with declustering in the mass spectrometer inlet, protein diameters determined by mobility measurements would be less than the protein sizes at the end of solvent evaporation and ion emission.

Given that protein diameter measurements give questionable results, protein diameters were calculated by two methods. First, the diameter measurements of Bacher et al.[33] and Kaddis et al.[34], were used, and a density (r) of 0.57 g cm^{-3} was used to determine the diameter of proteins not measured previously. Second, $\rho = 1.0$ g cm^{-3} was used for all proteins, which is greater than the largest gas phase protein densities measured previously[61], and is a suitable upper limit of the protein density. Using the upper limit does not invalidate the proposed mechanism of macromolecular ESI for native-state proteins, as will be shown later; rather the protein density affects the scaling between protein diameter and molecular weight.

RESULTS & DISCUSSION

We compare results for native-state and denatured proteins with the proposed mechanism of ESI. The diameters and measured mean charge states of the proteins are shown in Table 1. Column headers in the “Measured Mean Charge State” section denote the electrolyte used in protein solutions for each measurement.

Native-State Proteins

Previous observations are that the native-state conformations for many proteins, including those studied here, are maintained in aqueous NH_4Ac[3] and TEAB[62] Selected mass spectra obtained by using non-denaturing solutions are shown in Figure 2, and the mean charge states of all measured proteins with NH_4Ac as an electrolyte and TEAB as an electrolyte as a function of gas phase protein diameter are shown in Figures 3 and 4, respectively (with $\rho = 0.57$ g cm^{-3} in Figures 3a and 4a, and $\rho = 1.0$ g cm^{-3} in Figures 3b and 4b). Error bars for measured mean charge states represent the standard deviation of each protein's charge distribution, rather than the standard deviation of repeated measurements of the mean charge, which varied a negligible amount between experimental trials. Shown also are the mean charge states measured as sprayed from aqueous 10 mM ammonium acetate by Kaltashov and Mohimen[3] who used a double focusing magnetic sector instrument for mass measurement. The mean charge states for proteins measured here are in excellent agreement with those from previous studies utilizing ammonium or triethylammonium salts as electrolytes[3, 21, 22], showing that protein charge states are not strongly influenced by the type of mass spectrometer used in making measurements.

Conversely, the electrolyte used in the ESI solvent does affect the measured charge distributions, as seen not only in the mass spectra but also in the mean charge state versus protein diameter curves. Mean protein charge states were higher with aqueous NH_4Ac than they were with aqueous TEAB, but all were lower than the Rayleigh charge limit of water droplets. With both electrolytes, the average number of charges on each protein is proportional to the square of the gas-phase protein diameter. As noted in our preliminary communication[30], these data strongly support the proposed theory of ESI for macromolecules.

The electric field on the surface of an ion emitting droplet, E^*, should be independent of the droplet size and the protein size. Fitted values of E^* based on protein charge distribution measurements (Figures 3 and 4) show that a shift in E^* occurs at diameters of ~ 5 nm with $\rho = 0.57$ g cm^{-3} or at ~ 4 nm with $\rho = 1.0$ g cm^{-3} for ESI from aqueous NH_4Ac. This shift agrees well with the proposal that multiple charge carrier types are present in electrospray droplets when NH_4Ac is the electrolyte. As this shift was observable in two independently conducted studies, it is presumably due to the formation of charge-carrying ammonium acetate-based clusters and not the presence of impurities, which would likely not have been present in equal concentrations in both studies. The precise speciation of charge carriers, however, cannot not be determined from the data presented here, and further research will be necessary to verify the origin in shifts in E^* .

Although these native state protein measurements strongly support the assertion that protein charging is determined by charge-carrier speciation, measured values of E^* and diameters at which shifts in E* occur are a function of the gas-phase protein density. A priori prediction of the number of charges on a protein in ESI using a given electrolyte is hindered by the uncertainties in protein density and by the lack of knowledge of charge carrier speciation within droplets. As demonstrated by the agreement between the data measured here and those of Kaltashov and Mohimen, however, once charge-distribution measurements are made for a given electrolyte-solvent combination in ESI, E^* and shifts in E^* can be determined for ion-emitting droplets and used for quantitative predictions of charge-state measurements. This “calibration” technique can be performed by using any reasonable estimate of the gas-phase protein density, so long as the assumed protein density is used consistently.

Using measured data, we employed the charge carrier emission theory to predict the mass to charge (m/z) ratio at which an analyte of known mass will be detected. For mega and giga-Dalton analytes[63], the electric-field strength necessary to cause a droplet of similar size to fission is typically less than E^* of the least solvated charge carrier in the droplet. Therefore, charge-carrier emission does not occur from such droplets, and the Rayleigh limit determines the maximum number of charges on large analytes, as was previously proposed [5]. As droplets decrease in size owing to solvent evaporation, charge emission may begin to occur. The transition from Rayleigh-limited to ion-emission-governed charging can be predicted from the dimensionless ratio θ:

$$\theta = E * \left(\frac{\varepsilon_0 D}{8\sigma}\right)^{1/2} \quad (2)$$

where D is the diameter of the analyte, and σ is the solvent surface tension. For θ greater than unity, ion emission is not favored over Coulombic fission, and charging is Rayleigh-limited. For θ less than unity, the charge on an analyte will still be less than the Rayleigh limit, but the charge is determined by charge-carrier emission in accordance with the theory described here. Figure 5 shows the predicted mass-to-charge ratio of various analytes as a function of their mass for ESI from aqueous NH_4Ac (solid line) and aqueous TEAB (dashed line) with $\rho = 1.0$ g cm^{-3}. Transitions from Rayleigh-limited to ion-emission-controlled charging are indicated, and oscillations in the curve are due to the discrete nature of electric charge. For ESI from the two electrolyte systems, proteins with masses less than 100 kDa have θ less than unity, and their charge state is determined by charge-carrier emission. It must be noted, however, that the predicted diameter corresponding to the onset of charge-carrier emission is influenced somewhat by choice of protein density in the determination of E^*, again highlighting the importance of knowing the gas-phase protein density.

Gas-phase Proton Exchange

The fact that protein charge state is influenced by the type of electrolyte used in ESI does not preclude other mechanisms influencing the charge on native-state proteins. In previous studies[22, 64-66], it was suggested that gas-phase acid-base chemistry occurring between solute vapor and basic surface sites on the protein determine the charge state in ESI. It is known that the addition of chemical species with high gas-phase basicity reduces the charge on electrosprayed proteins[41]. For quantitative charge-state prediction, it is critical to determine whether charge-carrier emission or gas-phase proton exchange is influencing protein charging. In the case when charging is governed by charge-carrier emission, a macromolecule is a passive object; it merely accepts excess charge after solvent evaporation and ion emission cease, and only an estimate of the macromolecule's size is needed for charge-state prediction. Charge-state prediction based on a gas-phase proton exchange mechanism requires detailed understanding of macromolecular structure and the gas-phase basicity of exposed surface sites, making calculation of mean charge states and *m/z* limits (e.g., as done for Figure 5) difficult.

Proteins and macromolecules encapsulated in droplets with dissimilar charge carrier chemical compositions will have different charge states if charge state is determined by charge-carrier emission. In ESI from a mixture of electrolytes, it is well documented that Coulombic fissions can separate electrolytes from one another[67, 68]. The first several droplet fissions will create progeny droplets that are concentrated in the less-solvated, surface-active species. Later fissions occur when the parent droplet is depleted of surface-active species and the progeny droplets become enriched in more solvated electrolytes. Macromolecular ions in ESI arise from progeny droplets[37, 69]; thus, ESI using mixed (multiple) electrolytes should give rise to multiple droplet compositions and multi-modal protein charge-state distributions, if charge carrier emission is in fact governing protein charging. Conversely, gas-phase proton exchange presumably occurs after solvent and volatile electrolyte evaporation cease. Should gas-phase proton exchange affect protein charging, all macromolecular ions would be charged similarly owing to collisions with gas-phase electrolyte molecules (or species introduced separately[70]), regardless of the chemical composition of the droplets encapsulating them.

ESI mass spectra of native-state proteins in a mixed electrolyte of aqueous 5 mM NH_4Ac and 5 mM TEAB were measured (selected mass spectra are shown in Figure 6). All charge-state distributions were broad and appeared to be linear combinations of mass spectra measured in 10 mM aqueous TEAB and 10 mM aqueous NH_4Ac (c.f., Figures 3 and 4). The bimodal nature of these mass spectra indicates that gas-phase reactions between proteins and solute vapor do not substantially affect protein charge states. This is presumably due to the short time scale over which protein ions migrate into a mass spectrometer and the minute concentrations of solute vapor that are produced by ESI. In previous studies[41, 70], vapor of high gas-phase basicity was mixed with electrosprayed proteins for longer times than are typical in ESI-MS, and it was found that protein charge states are reduced below those observed in typical ESI-MS experiments without the additional introduction of such vapor[20, 22, 66]. Therefore, gas-phase decharging can occur under appropriate experimental conditions. Decharging, however, requires use of an external vapor source, as the partial pressures required to cause this reduction are orders of magnitude higher than is encountered normally for electrospraying proteins. The experiments performed here and reported previously thus support the theory that charge-carrier emission determines protein charge states and suggest that in most ESI-MS experiments, the effects of gas-phase proton exchange on charging are minimal.

Electrospray from Acidic and Basic Solutions

Often proteins are electrosprayed from highly acidic or basic solutions. Under these conditions, proteins may denature, giving up some tertiary and secondary structure and making them structurally similar to flexible polymer chains. The mean charge states from positive ESI mass

spectra, measured in aqueous HAc (pH = 2.1) and aqueous NH_4OH (pH = 11.5), are shown as a function of protein diameter (calculated by assuming a density of 1.0 g cm^{-3}) in Figure 7. For comparison, mean charge states of known native-state proteins with aqueous NH_4Ac are also shown. For ESI from solutions of either pH, the mean charge states for most measured proteins are slightly higher when the protein is at non-neutral pH as compared to when they are in neutral solution. A small increase in protein sizes would be expected to accompany some degree of denaturation[5]. Furthermore, the measured charge states do not differ substantially from the predicted ones on the basis of charge carrier field emission for most proteins (although note that with HAc as an electrolyte, the E^* for charge carrier emission may high enough that $\theta > 1.0$ for the proteins measured here).

For several proteins, however, electrospray from a low pH solution causes a large increase in the measured mean charge state. This shift is sufficiently large that the measured mean charge states of these proteins are greater than the Rayleigh limit of a water droplet of similar volume to the protein; hence these proteins are "supercharged[1]". A robust theory explaining the mechanism of ESI for macromolecules needs to account also for the phenomenon of supercharging. The key assumption in the proposed model of macromolecular ESI is that the excess surface-charge carriers in a droplet are small electrolyte and solvent ions, whereas the macromolecule resides in the droplet's interior. Therefore, charge-carrier emission from a droplet occurs unimpeded by the presence of a macromolecule and after desolvation, the remaining excess charges reside on the macromolecule, irrespective of the surface charge on the macromolecule in solution[71]. Compact, native state proteins meet the requirements of this assumption.

Partially or fully denatured proteins in basic solutions, near or above their isoelectric point, should also reside in the interior of positively charged droplets, as they are either neutral or negatively charged. Denatured proteins in acidic solutions far below their isoelectric point, however, may not necessarily reside within the interior of positively charged nanodroplets. They instead may reside partially on the surface of a charged nanodroplet and carry part of the droplet excess charge. Complete desorption of a denatured protein (or polymers with linear chains), residing on the surface of charged nanodroplet was proposed in the IEM of macromolecules[8, 9]. Complete desorption would not be, however, an energetically favorable process, as not all protein segments are charged, even in highly acidic solutions.

We propose here that supercharging occurs in positive-ion ESI for some proteins that denature in acidic solutions (and would also occur in negative-ion ESI for proteins that denature in basic solutions) because partial desorption of less solvated, charged segments of the denatured protein can occur. Charge-carrier emission and desorption are competitive processes. As the solvent in a droplet evaporates, partial desorption of a macromolecule on the droplet surface may be favored over emission of charge carriers composed of electrolyte and solvent. After partial desorption, the macromolecule would then "snake" in and out of the droplet. Charged segments protruding from the droplet surface would not contribute to the excess surface charge. Thus, denatured proteins may have charge states higher than the Rayleigh limit of a droplet of similar volume to that of the protein.

Although the occurrence of partial macromolecular desorption is not described explicitly by the theory of ESI proposed here, it does fit well within the kinetics context of charge-carrier emission. There is strong evidence that some small polypeptides and peptide clusters can exist as charge carriers in ESI droplets[72], and their emission will be preferred over that of charge-carrying electrolyte and solvent clusters. Therefore, the charge state of supercharged proteins is dependent on the chemical compositions of the protein and the droplet. Data show that supercharging is more prevalent for larger proteins. Larger proteins have a higher probability

of containing poorly solvated, charged segments and, therefore, are more likely to become supercharged than are smaller proteins, which are less likely to contain desorbing segments.

Low-Mass Analyte MS and Charge Emission Kinetics

Charge-carrier field emission governs not only charging of macromolecules, but also the ionization rates and ionization efficiencies of low-mass analytes. These latter analytes, commonly encountered in metabolomics and environmental systems[73], are likely to be charge carriers in nanodroplets. For mixtures of low-mass analytes, the E^* for each determines its ionization rate and to what extent it is emitted in competition with other analytes. E^*, in turn, is dependent upon the solvation energy, $G_{s,i}$, of the analyte ionized in solution. The relationship between E^* and $G_{s,i}$ can be determined by examining the governing equations for solvent evaporation and charge emission from a droplet. The rate of solvent evaporation for nanodroplets is determined by equation [3]:

$$\frac{dn_s}{dt} = -\frac{D^2}{\left(2\pi m_g k_b T\right)}^{1/2} P_s \exp\left(\frac{4\sigma v_m}{k_b T D}\right) \tag{3}$$

where n_s is the number of solvent molecules in the droplet, v_m is the solvent molecular volume, D is the droplet diameter ($D = [6v_m n_s/\pi]^{1/3}$), m_g is a mass of a bath-gas molecule, k_b is the Boltzmann constant, T is the electrolyte temperature of the surrounding bath gas, and p_s is the saturation vapor pressure of the solvent. Kinetic expressions describing the emission rate of charged species from a charged nanodroplet were originally developed by Iribarne and Thomson[12] and later refined by Fernandez de la Mora and coworkers[15, 31, 42]. The change in number of charge carriers of species i can be determined approximately from equation [4]:

$$\frac{dn_i}{dt} = -\left(\frac{k_b T}{h}\right) \exp\left(\frac{G_E - G_{s,i}}{k_b T}\right) \sum_{i=1}^{j} n_i \tag{4}$$

where n_i is the number of charge carriers of species i on the droplet surface, h is Planck's constant, j is the total number of different types of charge carriers in the droplet, and G_E is the electrical surface energy of the droplet, given by equation [5]:

$$G_E = \left(\frac{e^3 E}{4\pi\varepsilon_0}\right)^{1/2} \tag{5}$$

where E is the electric field on the droplet surface ($E = ne/\varepsilon_0 \pi D^2$). Equation [4] is only valid when n_i is constant for all i, and, thus, is not amenable to direct integration. The Direct Monte Carlo technique[74], however, can be used to solve these equations in a coupled manner to determine the number of excess charges on a droplet as a function of its diameter. To determine the relationship between $G_{s,i}$ and E^*, we generated charge-state versus droplet-diameter curves for $i = 1$ and for varying solvation energies. The electric field E on the droplet was determined for each point in the simulation, and E* was taken as the average E over the course of the simulation (see Figure 8a for the E* versus $G_{s,i}$ curves for both water and methanol at 50 °C). E varies little over the course of the simulation, indicating that E^* is in fact a constant for droplets emitting a single type of charge carrier. The curves are insensitive to changes in temperature, and the linear relationship between solvation energy and the square root of E^* indicates that ion emission occurs at a critical free energy difference between the ion solvation energy and droplet surface electric energy.

If the speciation and solvation energy of all charge carriers in a given electrolyte-solvent system were known[44], then charge-state versus droplet-diameter curves, and subsequently predicted charge-state versus macromolecular-diameter curves, can be generated without the need for prior measurements. As an example, Figure 8b shows the results of a Monte Carlo simulation

for a droplet with two charge carriers with solvation energies of 2.46 eV (21 charges originally) and 2.66 eV (9 charges originally). The corresponding E^* values for charges with solvation energies of 2.46 eV and 2.66 eV are 2.95 V/nm and 3.53 V/nm, respectively. The charge-state versus droplet-diameter curves for the aforementioned E^* values are also shown in Figure 8b. As expected, the less solvated charge carrier emits first from the droplet when the droplet electric field is approximately 2.95 V/nm. After the droplet depletes of the less solvated charge carrier (at charge state $n = 9$), its electric field increases to 3.53 V/nm, allowing the more solvated charge carrier to be emitted. Preferential ion emission of less solvated species, therefore, follows directly from the kinetics of solvent evaporation and ion emission.

CONCLUSIONS

The basic tenets of the model of ESI reported here are that macromolecules reside in the interior of ESI droplets and that small solvent and electrolyte ions carry the excess surface charge of droplets. Accordingly, the charge state of a macromolecule emitted in ESI is a function of its unsolvated size and the solvation energy of the charge carriers in the droplet. Macromolecules are passive objects in this model; charge-carrier emission kinetics determine the charge state on evaporating droplets, and charge is transferred to macromolecules as solvent evaporation nears completion. ESI of native-state proteins from aqueous solutions containing different electrolytes and electrolyte mixtures provide strong support for this model. Its development follows directly from known kinetic expressions for ion emission and solvent evaporation from charged nanodroplets. The model appears to be applicable to most proteins measured in ESI-MS, with the exception “supercharged” proteins, formed in positive-ion ESI from highly acidic solutions.

This model of ESI resolves differences between the previously proposed ion-emission mechanism and charge-residue mechanism for macromolecular ions. Future work will be necessary, however, to examine the chemical nature of charge carriers in electrospray droplets and to determine if protein charge states can be determined a priori through knowledge of charge carrier speciation. With such future developments, applications of this model should allow for quantitative, a priori predictions of ESI mass spectra, ionization rates, and ionization efficiencies for analytes in proteomics, metabolomics and other analytical systems where electrospray ionization is utilized.

ACKNOWLEDGEMENTS

C.J.H. acknowledges support from a National Science Foundation graduate research fellowship. The authors thank Professor Juan Fernandez de la Mora and Sergio Castro (Yale University) for useful discussions on the kinetics of ion emission. Partial support of the research comes from the National Centers for Research Resources of the NIH (Grant 2P41RR000954).

REFERENCES

(1). Iavarone AT, Williams ER. Journal of the American Chemical Society 2003;125:2319–2327. [PubMed: 12590562]

(2). Jiang JK, Hogan CJ, Chen DR, Biswas P. Journal of Applied Physics 2007;102:034904.

(3). Kaltashov IA, Mohimen A. Analytical Chemistry 2005;77:5370–5379. [PubMed: 16097782]

(4). Dole M, Mack LL, Hines RL, Mobley RC, Ferguson LD, Alice MB. Journal of Chemical Physics 1968;49:2240–2249.

(5). Fernandez de la Mora J. Analytica Chimica Acta 2000;406:93–104.

(6). Kebarle P, Peschke M. Analytica Chimica Acta 2000;406:11–35.

(7). Zhan D, Rosell J, Fenn JB. Journal of the American Society for Mass Spectrometry 1998;9:1241–1247.

(8). Fenn JB, Rosell J, Meng CK. Journal of the American Society for Mass Spectrometry 1997;8:1147–1157.

(9). Fenn JB. Journal of the American Society for Mass Spectrometry 1993;4:524–535.

(10). Wong SF, Meng CK, Fenn JB. Journal of Physical Chemistry 1988;92:546–550.

(11). Thomson BA, Iribarne JV. Journal of Chemical Physics 1979;71:4451–4463.

(12). Iribarne JV, Thomson BA. Journal of Chemical Physics 1976;64:2287–2294.

(13). Ku BK, Fernandez de la Mora J. Journal of Physical Chemistry B 2004;108:14915–14923.

(14). Ku BK, Fernandez de la Mora J. Journal of Physical Chemistry B 2005;109:11173–11179.

(15). Loscertales IG, Fernandez de la Mora J. Journal of Chemical Physics 1995;103:5041–5060.

(16). Gamero-Castano M, Fernandez de la Mora J. Journal of Mass Spectrometry 2000;35:790–803. [PubMed: 10934433]

(17). Gamero-Castano M, Fernandez de la Mora J. Journal of Chemical Physics 2000;113:815–832.

(18). Kebarle P. Journal of Mass Spectrometry 2000;35:804–817. [PubMed: 10934434]

(19). Peschke M, Blades A, Kebarle P. Journal of the American Chemical Society 2002;124:11519–11530. [PubMed: 12236767]

(20). Felitsyn N, Peschke M, Kebarle P. International Journal of Mass Spectrometry 2002;219:39–62.

(21). Nesatyy VJ, Suter MJF. Journal of Mass Spectrometry 2004;39:93–97. [PubMed: 14760619]

(22). Catalina MI, van den Heuvel RHH, van Duijn E, Heck AJR. Chemistry-a European Journal 2005;11:960–968.

(23). Tolic LP, Anderson GA, Smith RD, Brothers HM, Spindler R, Tomalia DA. International Journal of Mass Spectrometry 1997;165:405–418.

(24). Kuprowski MC, Konermann L. Analytical Chemistry 2007;79:2499–2506. [PubMed: 17288464]

(25). Dobo A, Kaltashov IA. Analytical Chemistry 2001;73:4763–4773. [PubMed: 11681449]

(26). Frimpong AK, Abzalimov RR, Eyles SJ, Kaltashov IA. Analytical Chemistry 2007;79:4154–4161. [PubMed: 17477507]

(27). Konermann L, Douglas DJ. Rapid Communications in Mass Spectrometry 1998;12:435–442. [PubMed: 9586231]

(28). Konermann L, Douglas DJ. Journal of the American Society for Mass Spectrometry 1998;9:1248–1254. [PubMed: 9835071]

(29). Konermann L, Douglas DJ. Biochemistry 1997;36:12296–12302. [PubMed: 9315869]

(30). Hogan CJ, Carroll JA, Rohrs HW, Biswas P, Gross ML. Journal of the American Chemical Society 2008;130:6926–6927. [PubMed: 18461930]

(31). Gamero-Castano M, Fernandez de la Mora J. Analytica Chimica Acta 2000;406:67–91.

(32). Fernandez de la Mora J, Thomson BA, Gamero-Castano M. Journal of the AmericanSociety for Mass Spectrometry 2005;16:717–732.

(33). Bacher G, Szymanski WW, Kaufman SL, Zollner P, Blaas D, Allmaier G. Journal of Mass Spectrometry 2001;36:1038–1052. [PubMed: 11599082]

(34). Kaddis CS, Lomeli SH, Yin S, Berhane B, Apostol MI, Kickhoefer VA, Rome LH, Loo JA. Journal of the American Society for Mass Spectrometry 2007;18:1206–1216. [PubMed: 17434746]

(35). Ruotolo BT, Giles K, Campuzano I, Sandercock AM, Bateman RH, Robinson CV. Science 2005;310:1658–1661. [PubMed: 16293722]

(36). Fernandez de la Mora J. Journal of Colloid and Interface Science 1996;178:209–218.

(37). Hogan CJ, Biswas P. Journal of the American Society for Mass Spectrometry 2008;19:1098–1107. [PubMed: 18554924]

(38). Znamenskiy V, Marginean I, Vertes A. Journal of Physical Chemistry A 2003;107:7406–7412.

(39). Hautreux M, Hue N, de Kerdaniel ADF, Zahir A, Malec V, Laprevote O. International Journal of Mass Spectrometry 2004;231:131–137.

(40). Clemmer DE, Hudgins RR, Jarrold MF. Journal of the American Chemical Society 1995;117:10141–10142.

(41). Gross DS, Schnier PD, RodriguezCruz SE, Fagerquist CK, Williams ER. Proceedings of the National Academy of Sciences of the United States of America 1996;93:3143–3148. [PubMed: 8610183]

(42). Labowsky M, Fenn JB, Fernandez de la Mora J. Analytica Chimica Acta 2000;406:105–118.

(43). Ude S, Fernandez de la Mora J. Journal of Aerosol Science 2005;36:1224–1237.

(44). Cech NB, Enke CG. Analytical Chemistry 2001;73:4632–4639. [PubMed: 11605841]

(45). Cech NB, Enke CG. Analytical Chemistry 2000;72:2717–2723. [PubMed: 10905298]

(46). Yang PX, Cooks RG, Ouyang Z, Hawkridge AM, Muddiman DC. Analytical Chemistry 2005;77:6174–6183. [PubMed: 16194076]

(47). Kaufman SL, Skogen JW, Dorman FD, Zarrin F, Lewis KC. Analytical Chemistry 1996;68:1895–1904.

(48). Hogan CJ, Kettleson EM, Ramaswami B, Chen DR, Biswas P. Analytical Chemistry 2006;78:844–852. [PubMed: 16448059]

(49). Lenggoro IW, Widiyandari H, Hogan CJ, Biswas P, Okuyama K. Analytica Chimica Acta 2007;585:193–201. [PubMed: 17386665]

(50). Fuchs NA. Geofis. Pura Appl 1963;51:185–193.

(51). Scalf M, Westphall MS, Smith LM. Analytical Chemistry 2000;72:52–60. [PubMed: 10655634]

(52). Fernandez de la Mora J, de Juan L, Liedtke K, Schmidt-Ott A. Journal of Aerosol Science 2003;34:79–98.

(53). Kaufman SL. Analytica Chimica Acta 2000;406:3–10.

(54). Gamero-Castano M, Fernandez de la Mora J. Journal of Aerosol Science 2000;31:757–772.

(55). Thomson BA. Journal of the American Society for Mass Spectrometry 1997;8:1053–1058.

(56). Laschober C, Kaddis CS, Reischl GP, Loo JA, Allmaier G, Szymanski WW. Journal of Experimental Nanoscience 2007;2:291–301.

(57). Hogan CJ, Biswas P. Journal of Aerosol Science 2008;39:432–440.

(58). Ude S, Fernandez de la Mora J, Alexander JN, Saucy DA. Journal of Colloid and Interface Science 2006;293:384–393. [PubMed: 16054154]

(59). Fernandez de la Mora J, de Juan L, Eichler T, Rosell J. Trac-Trends in Analytical Chemistry 1998;17:328–339.

(60). Mesleh MF, Hunter JM, Shvartsburg AA, Schatz GC, Jarrold MF. Journal of Physical Chemistry A 1997;101:968–968.

(61). Kaufman SL. Journal of Aerosol Science 1998;29:537–552.

(62). Lemaire D, Marie G, Serani L, Laprevote O. Analytical Chemistry 2001;73:1699–1706. [PubMed: 11338582]

(63). Van Den Heuvel RHH, Heck AJR. Current Opinion in Chemical Biology 2004;8:519–526. [PubMed: 15450495]

(64). Touboul D, Jecklin MC, Zenobi R. Journal of Physical Chemistry B 2007;111:11629–11631.

(65). Schnier PD, Gross DS, Williams ER. Journal of the American Society for Mass Spectrometry 1995;6:1086–1097.

(66). Peschke M, Verkerk UH, Kebarle P. European Journal of Mass Spectrometry 2004;10:993–1002. [PubMed: 15775058]

(67). Bakhoum SFW, Bogan MJ, Agnes GR. Analytical Chemistry 2005;77:3461–3465. [PubMed: 15924376]

(68). Tang KQ, Smith RD. Journal of the American Society for Mass Spectrometry 2001;12:343–347. [PubMed: 11281610]

(69). Tang KQ, Smith RD. International Journal of Mass Spectrometry 1999;187:97–105.

(70). Loo RRO, Smith RD. Journal of the American Society for Mass Spectrometry 1994;5:207–220.

(71). Carbeck JD, Severs JC, Gao JM, Wu QY, Smith RD, Whitesides GM. Journal of Physical Chemistry B 1998;102:10596–10601.

(72). Spencer EAC, Ly T, Julian RR. International Journal of Mass Spectrometry 2008;270:166–172.

(73). Richardson SD. Analytical Chemistry 2006;78:4021–4045. [PubMed: 16771539]

(74). Maisels A, Jordan F, Kruis FE, Fissan H. Journal of Nanoparticle Research 2003;5:225–235.

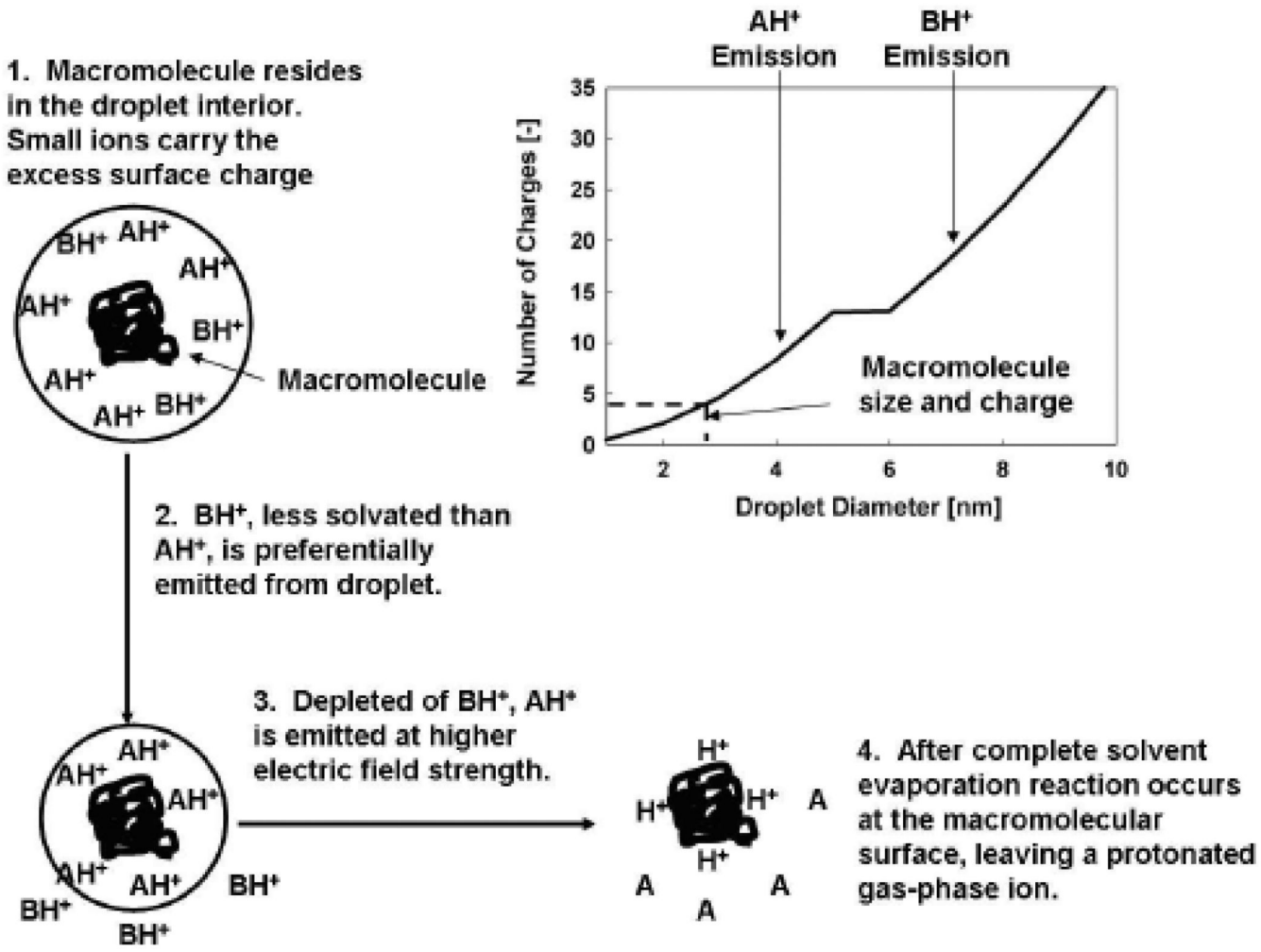

Figure 1.
Schematic representation of charge carrier emission from a macromolecule-containing, charged nanodroplet.

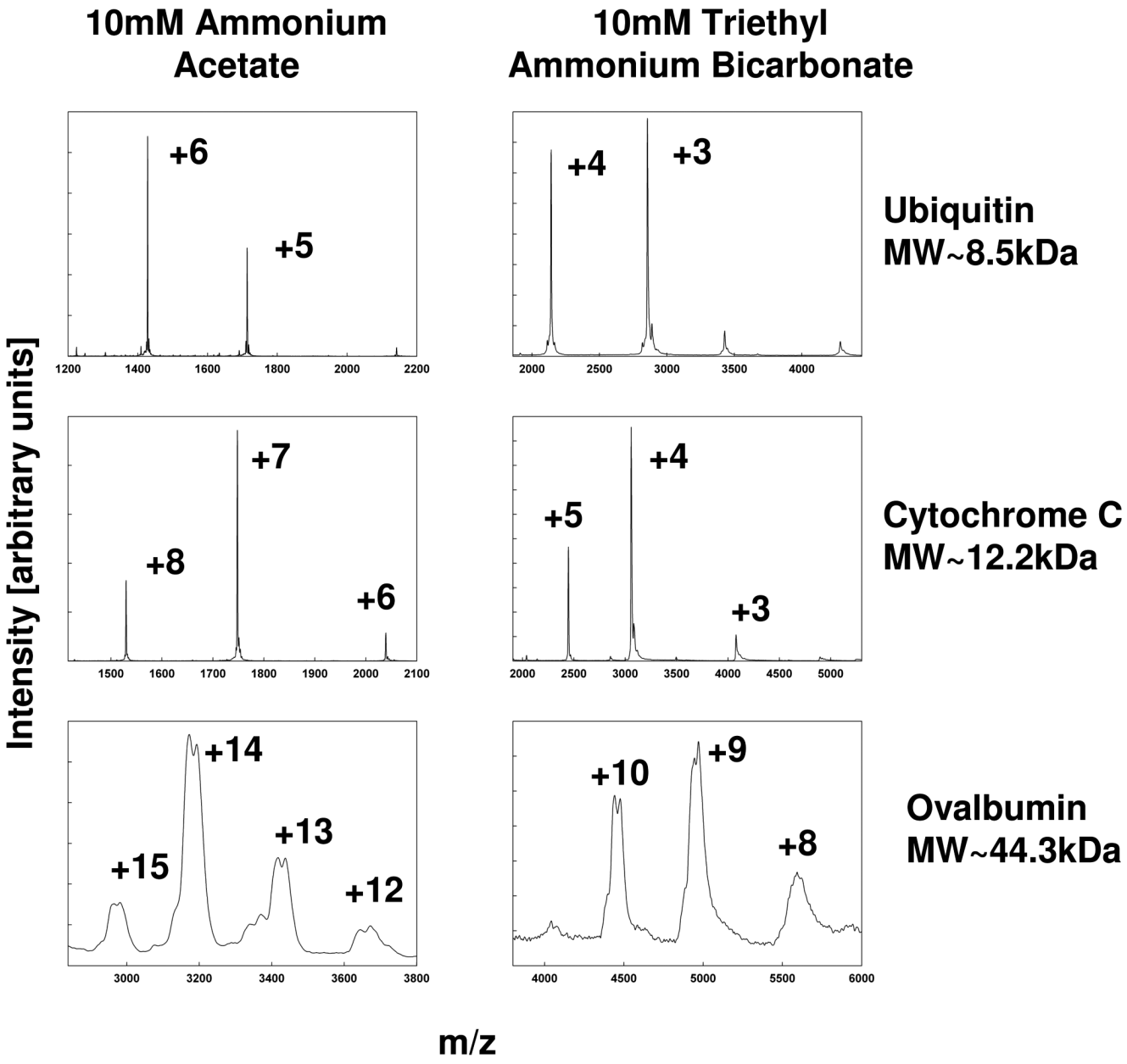

Figure 2.
Selected ESI mass spectra of native-state proteins; media were aqueous ammonium acetate and aqueous triethylammonium bicarbonate.

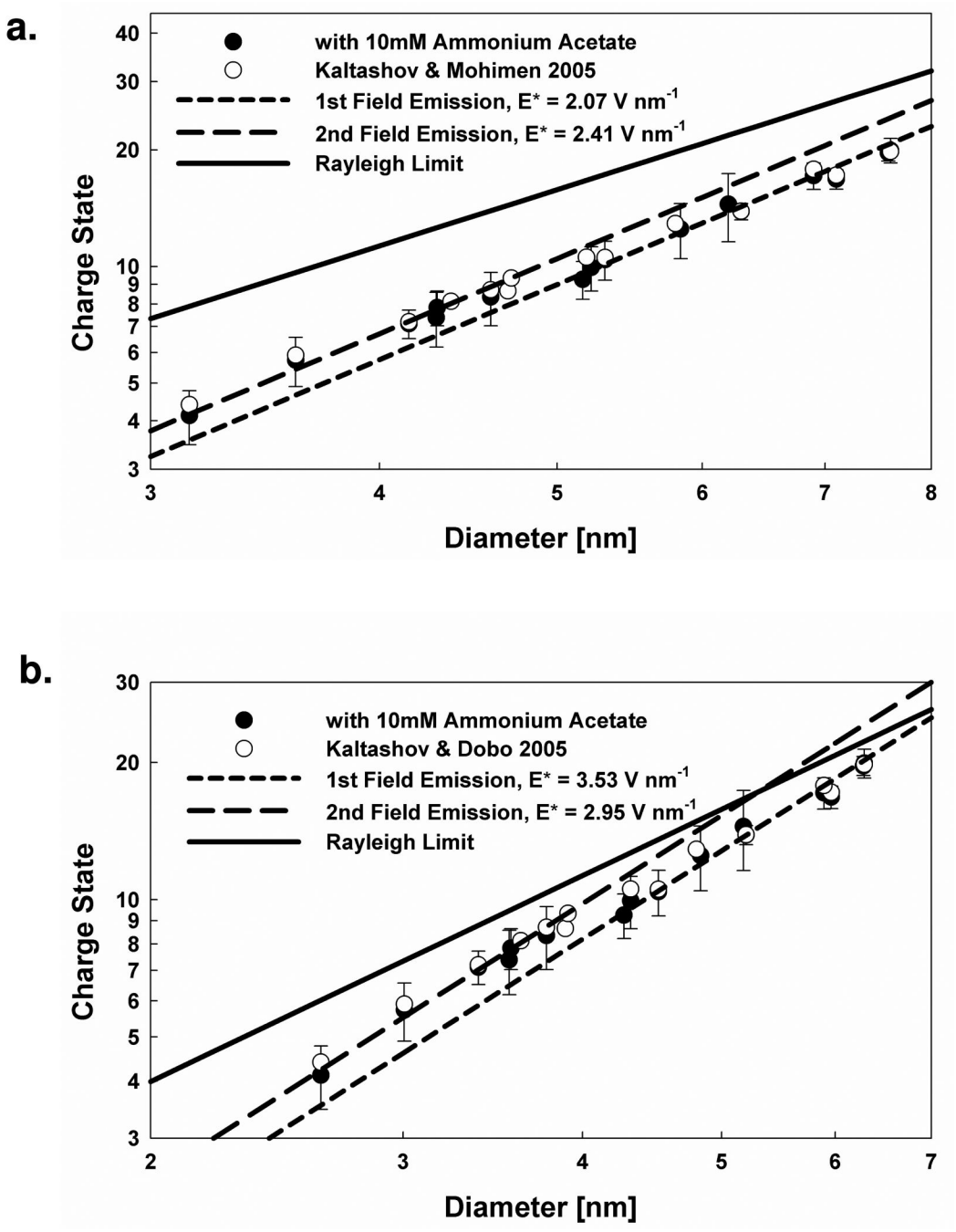

Figure 3.

Protein mean charge state as measured by ESI-MS in 10 mM aqueous ammonium acetate as a function of protein diameter calculated for protein densities of **a)** 0.57 g cm^{-3} and **b)** 1.00 g cm^{-3}.

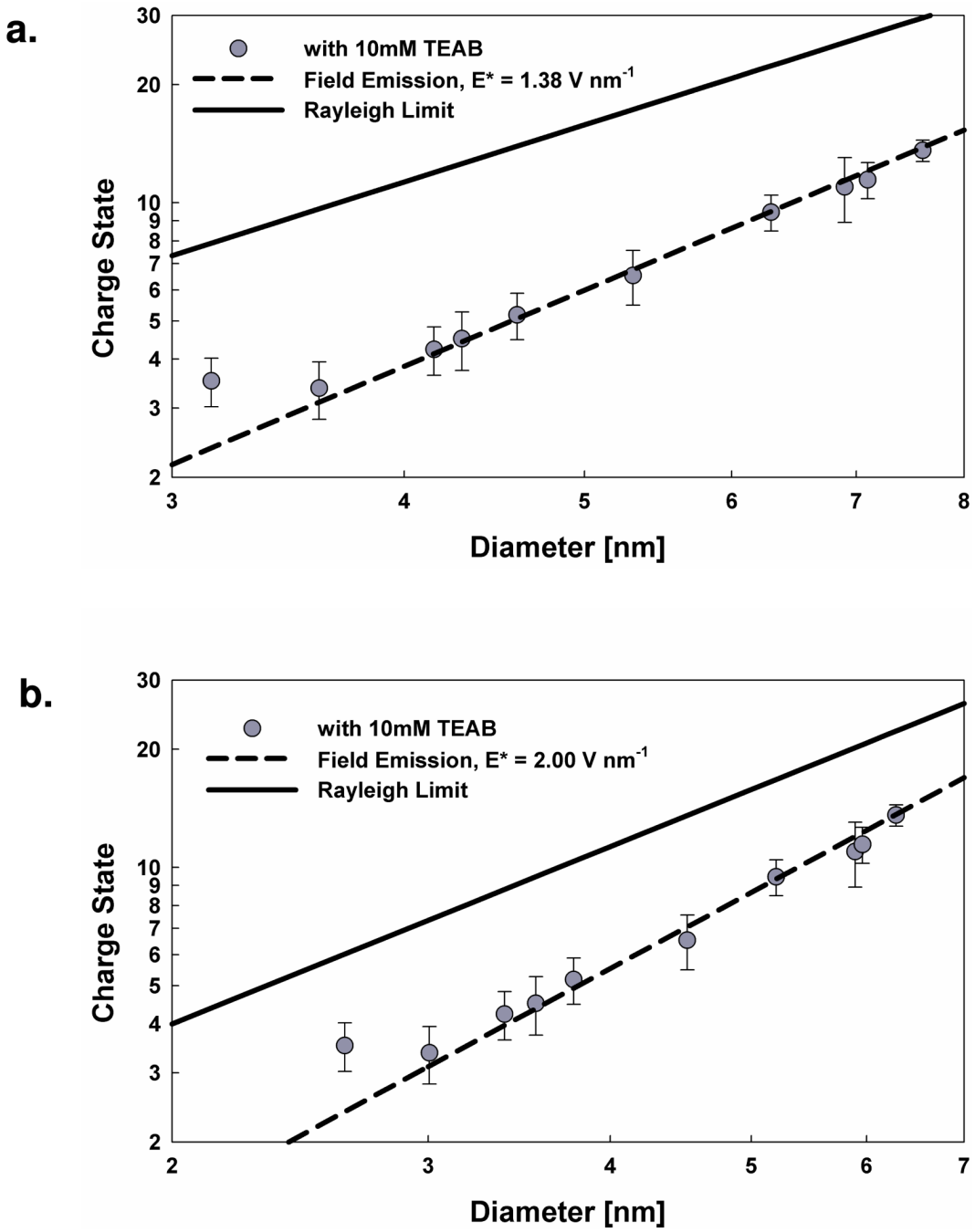

Figure 4.
Protein mean charge state as measured by ESI-MS in 10 mM aqueous triethylammonium bicarbonate as a function of protein diameter calculated for protein densities of **a)** 0.57 g cm^{-3} and **b)** 1.00 g cm^{-3}.

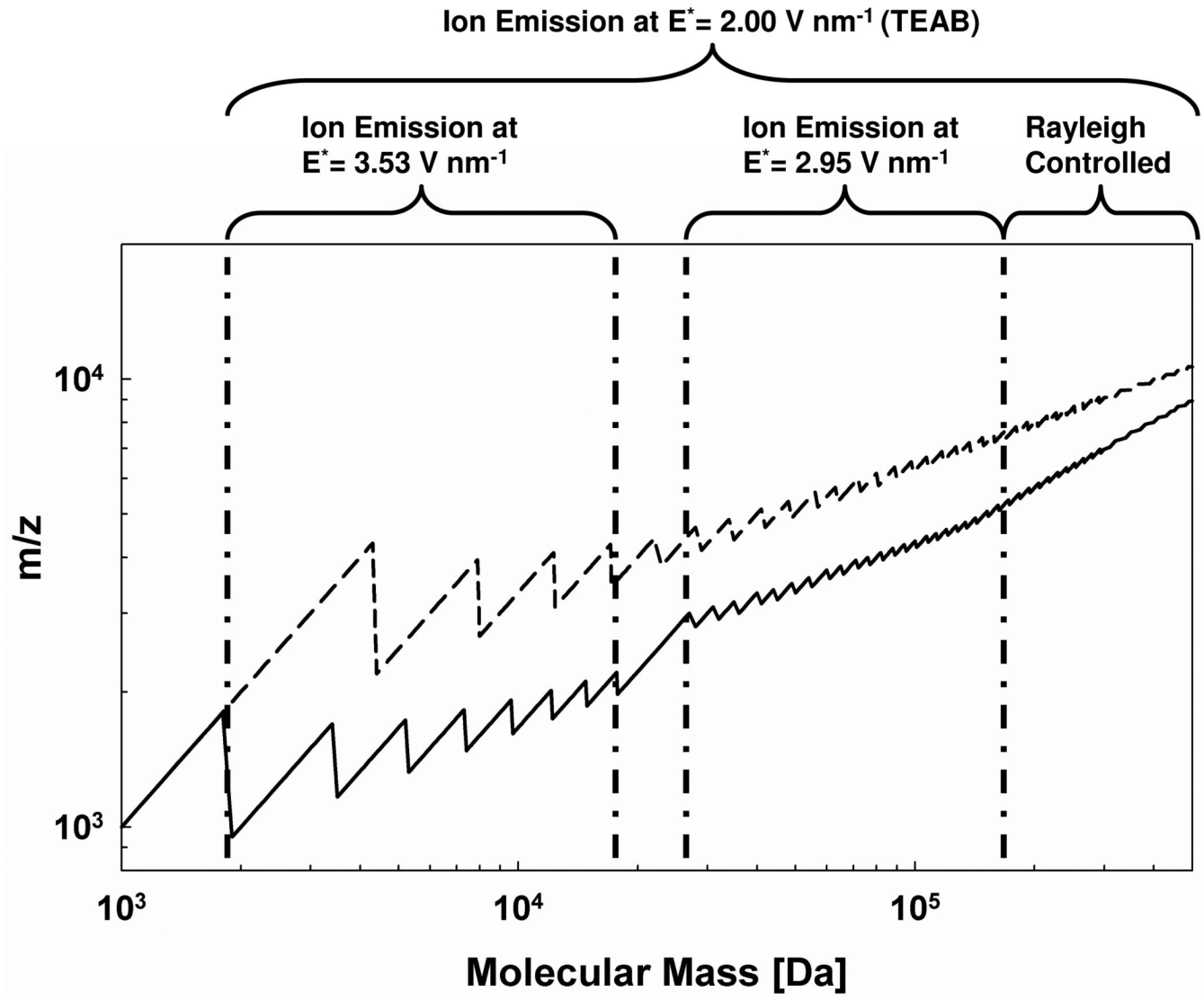

Figure 5.
Expected mass-to-charge ratio as a function of analyte mass for ESI from 10 mM aqueous ammonium acetate (solid line) and aqueous triethylammonium bicarbonate (dashed line) for an analyte with a density of 1.00 g cm^{-3}.

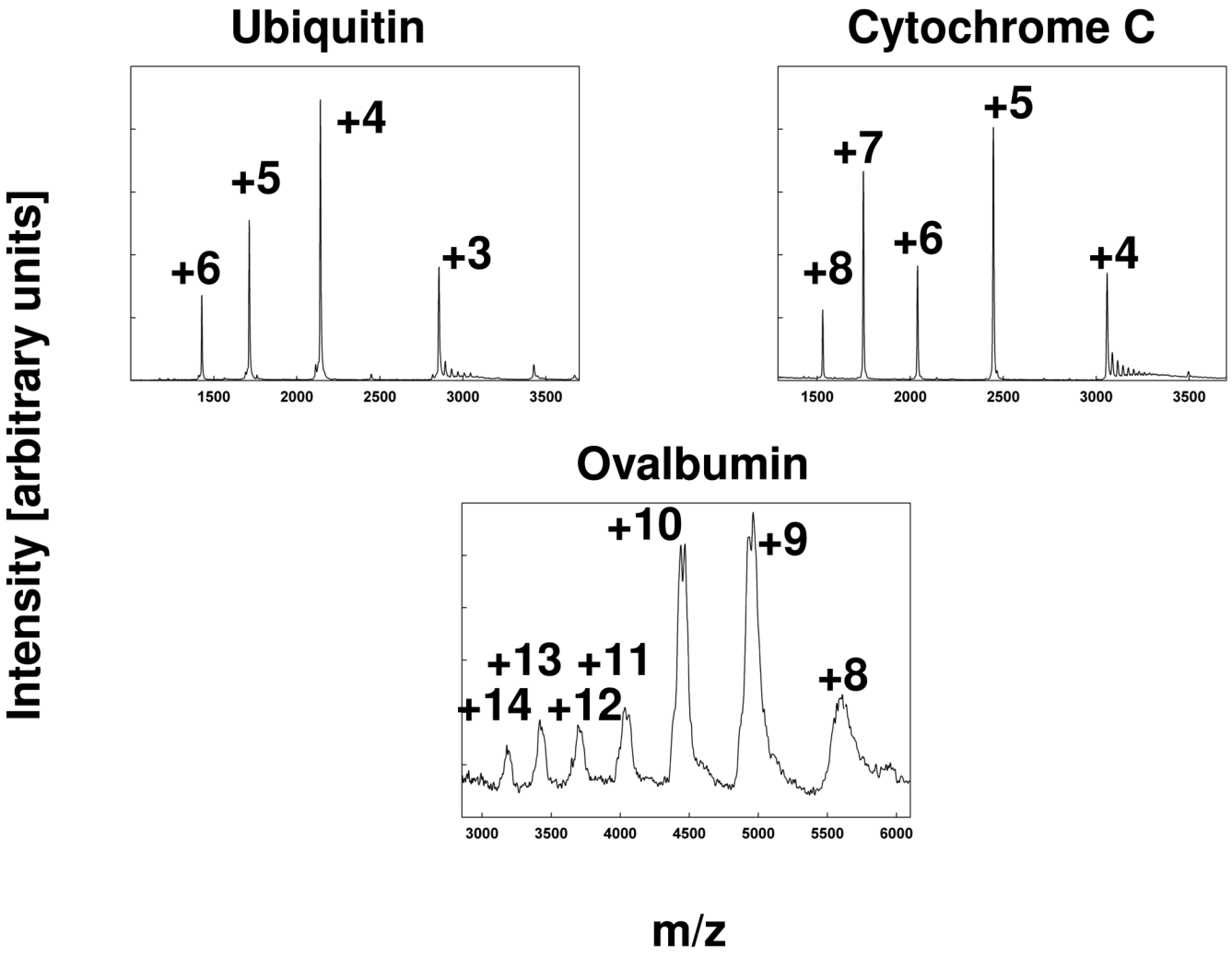

Figure 6.
Selected ESI mass spectra of native-state proteins; media were mixtures of aqueous 5 mM ammonium acetate and 5 mM triethylammonium bicarbonate.

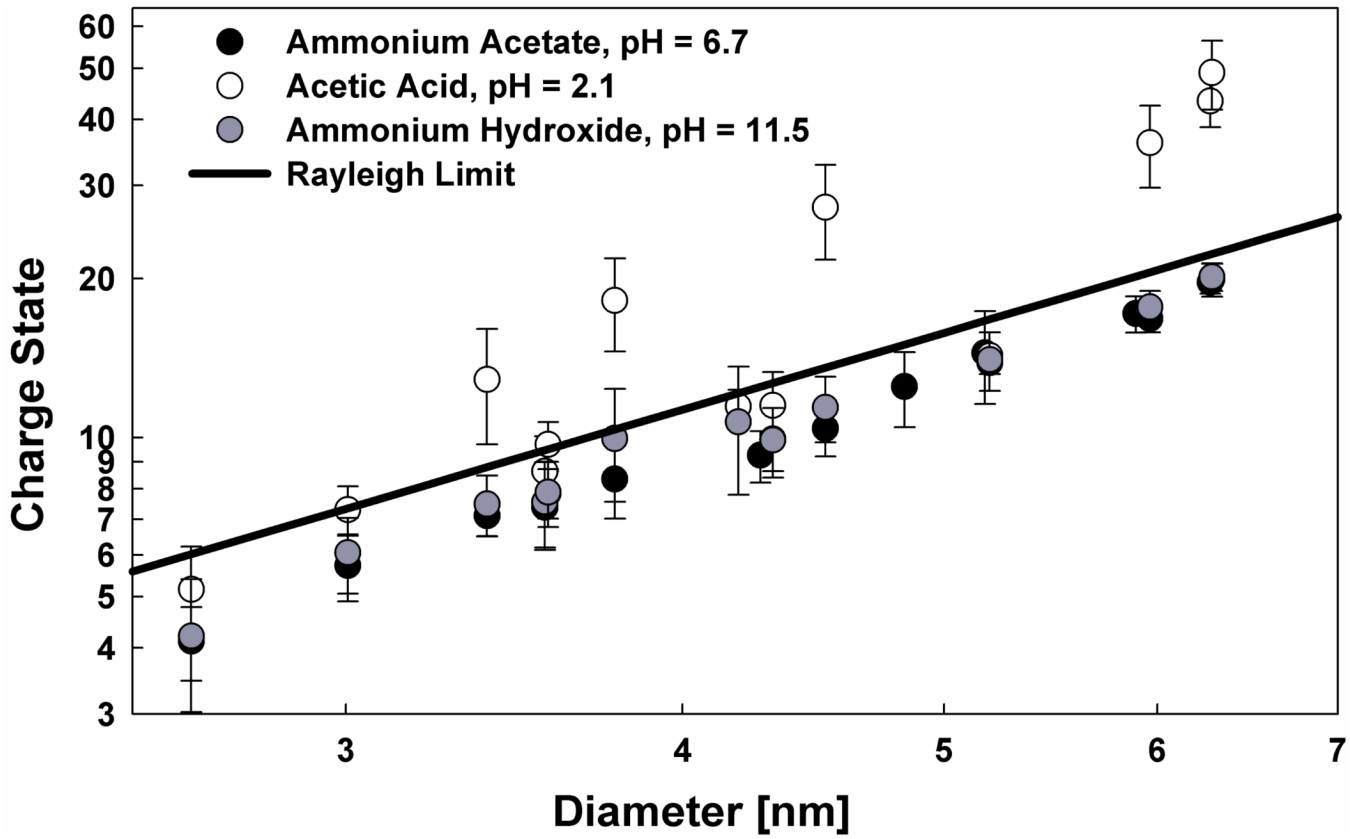

Figure 7.
Protein mean charge state measured by ESI-MS in aqueous ammonium acetate, acetic acid, and ammonium hydroxide as a function of protein diameter.

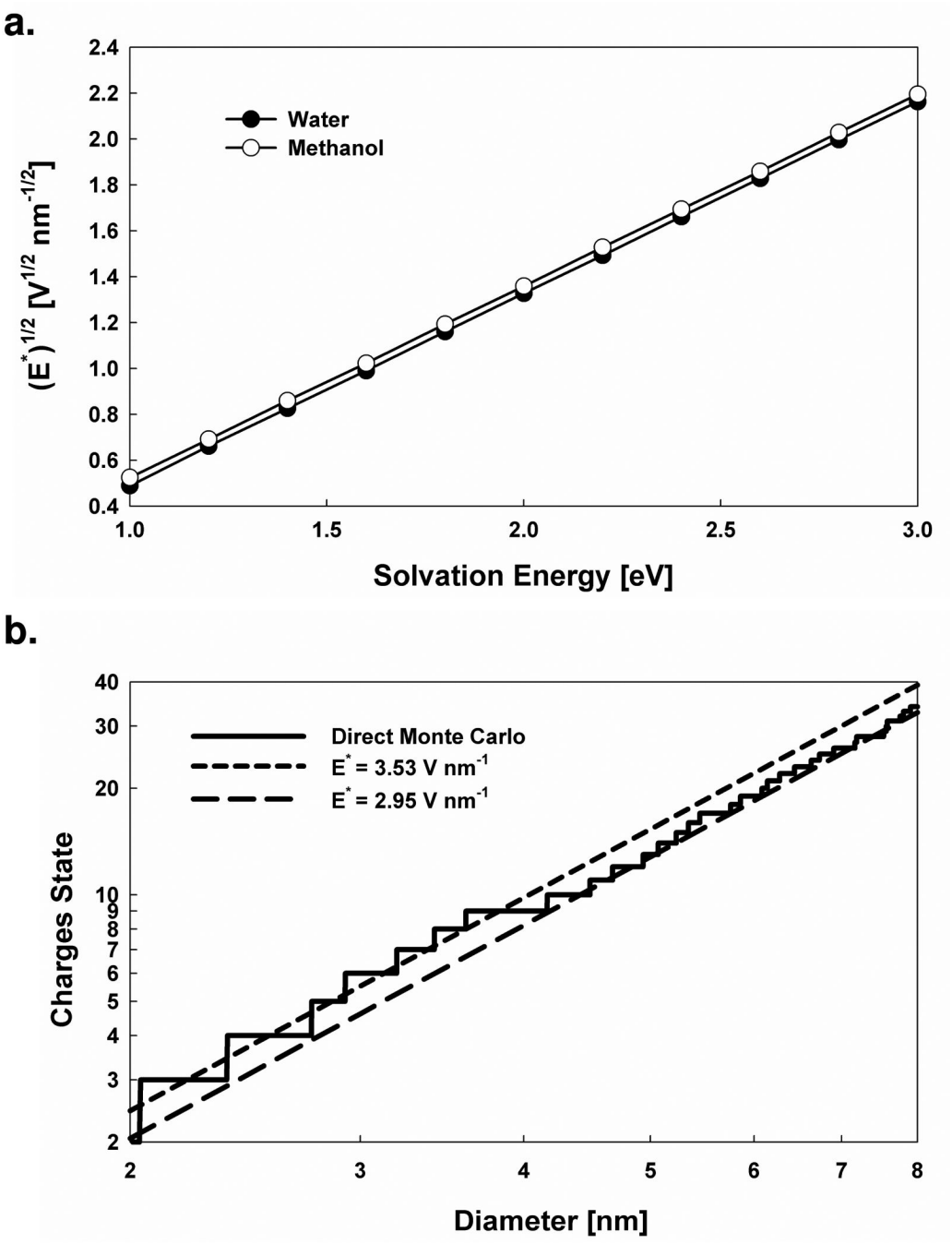

Figure 8.

a) Square of the critical field strength required for charge-carrier emission, E*, as a function of the charge carrier's solvation energy; results from direct Monte Carlo simulations. **b)** Theoretical charge state versus droplet diameter curve from direct Monte Carlo simulation for a charge-emitting nanodroplet containing two charge carriers with solvation energies of 2.46 eV (21 excess charges) and 2.66 eV (9 excess charges).

Table 1

Summary of calculated diameters for globular proteins; diameters were obtained by using two different densities and measured mean charge states in different aqueous media.

			Measured Mean Charge State (Standard Deviation)				
Protein	**Diameter (nm) ρ = 0.57 g cm^{-3}**	**Diameter (nm) ρ = 1.00 g cm^{-3}**	**10mM Ammonium Acetate**	**10mM Triethyl Ammonium Bicarbonate**	**Kaltashav & Mohimen (2005)**	**Aqueous Acetic Acid, pH = 2.1**	**Aqueous Ammonium Hydroxide, pH = 11.5**
Insulin	3.15[a]	2.63[c]	4.12 (0.65)	3.52 (0.50)	4.4	5.16 (1.06)	4.21 (1.19)
Ubiquitin	3.60[a]	3.01[c]	5.73 (0.83)	3.37 (0.56)	5.9	7.30 (0.78)	6.06 (0.99)
Cytochrome C	4.15[a]	3.38[c]	7.11 (0.60)	4.23 (0.59)	7.2	12.89 (3.18)	7.49 (0.99)
Lactalbumin	4.29[b]	3.56[c]	7.38 (1.19)	4.50 (0.76)	-	8.63 (1.42)	7.56 (1.43)
Lysozyme	4.30[a]	3.57[c]	7.83 (0.80)	-	-	9.71 (0.99)	7.89 (1.12)
CRABP I[x]	4.37[b]	3.62[c]	-	-	8.13	-	-
Myoglobin	4.60[a]	3.78[c]	8.34 (1.31)	5.18 (0.70)	8.7	18.19 (3.64)	9.96 (2.40)
β-lactoglobulin A	4.70[a]	3.89[c]	-	-	8.65	-	-
H-chain of Ferritin	4.72[a]	3.91[c]	-	-	9.33	-	-
Acylated Trypsin	5.16[b]	4.27[c]	9.25 (1.04)	-	-	11.46 (0.85)	10.71 (2.91)
Chymotrypsinogen	5.22[b]	4.32[c]	9.94 (1.30)	-	10.56	11.50 (1.81)	9.90 (1.49)
Carbonic Anhydrase	5.31[a]	4.52[c]	10.41 (1.19)	6.53 (1.04)	10.54	27.27 (5.55)	11.42 (1.62)
β-lactoglobulin A Dimer	5.80[a]	4.80[c]	-	-	12.9	-	-
G3PD[y]	5.84[b]	4.83[c]	12.49 (2.03)	-	-	-	-
Fetuin	6.20[a]	5.18[c]	14.47 (2.89)	-	-	-	-
Ovalbumin	6.30[a]	5.20[c]	13.87 (0.67)	9.46 (0.98)	13.89	14.30 (0.36)	14.05 (1.79)
Hemoglobin	6.90[a]	5.89[c]	17.15 (1.35)	-	17.8	-	-
Bovine Serum Albumin	7.10[a]	5.96[c]	16.79 (0.96)	11.44 (1.20)	17.2	36.11 (6.40)	17.67 (1.28)
Lactoferrin	7.58[a]	6.28[c]	19.66 (0.93)	-	-	-	-
Holotransferrin	7.60[a]	6.29[c]	19.93 (1.45)	13.58 (1.20)	19.8	49.06 (7.30)	20.14 (1.20)

[a] From Kaddis et al., 2007, J. Am. Soc. Mass Spectrom., 18:1206-1216

[b] From regression equation, Diameter (nm) = 0.1775Molecular Weight(kDa)^{33}

[c] From regression equation, Diameter (nm) = 0.1469Molecular Weight(kDa)^{33}

[x] Cellular Retinoic Acid Binding Protein I

[y] Glyceraldehyde 3-Phosphate Dehydrogenase